Periodic unrestricted Hartree-Fock study of corundumlike Ti_2O_3 and V_2O_3

M. Catti* and G. Sandrone
Dipartimento di Chimica Fisica ed Elettrochimica, Università di Milano, via Golgi 19, 20133 Milano, Italy

R. Dovesi
Dipartimento di Chimica Inorganica, Fisica e dei Materiali, Università di Torino, via Giuria 5, 10125 Torino, Italy
(Received 24 June 1996; revised manuscript received 17 December 1996)

The ground-state electronic and magnetic properties of rhombohedral Ti_2O_3 and V_2O_3 have been investigated by *ab initio* all-electron periodic Hartree-Fock calculations. Both unrestricted open-shell and restricted closed-shell methods have been employed, with basis sets of atomic orbitals represented by contracted Gaussian-type functions. The t_{2g} degeneracy of d electrons is removed by the rhombohedral field, giving rise to orbital ordering between a_{1g} and e_g^{π} levels. The self-consistent-field variational solutions are spin-polarized insulating states with single (a_{1g}) and double (e_g^{π}) electron occupations for Ti_2O_3 and V_2O_3, respectively. Conducting or semiconducting states, with different relative energies of a_{1g} and e_g^{π} bands, have also been obtained by changing the c/a ratio of the hexagonal unit cell. The charge transfer into e_g^{σ} levels is discussed and compared to the Cr_2O_3 and Fe_2O_3 behavior. [S0163-1829(97)06319-4]

I. INTRODUCTION

The recent progress in making available very efficient computational tools for calculating the electronic and magnetic properties of solids has led one to reconsider some classical series of isostructural transition-metal oxides. In particular, the periodic unrestricted Hartree-Fock (UHF) approach has been used to study a number of rocksalt-like oxides[1] and two of those with corundum structure, Fe_2O_3 and Cr_2O_3 (Refs. 2 and 3). A very successful achievement is the correct prediction of the least-energy antiferromagnetic structures of Fe_2O_3 ($R\bar{3}$) and Cr_2O_3 ($R3c$), among the subgroups of the $R3c$ corundum symmetry.[3] Some rocksalt and rutile-type oxides[4,5] have also been examined by methods based on density-functional theory (DFT), in its LAPW (linearized augmented plane waves)—LSDA (local spin density approximation) version.

Understanding the electronic behavior of such compounds has been a long-standing problem, because of the effects of exchange (spin-only correlation) and Coulomb-only electron correlation, which cause a simple one-electron picture of these solids to fail. Many advances, however, have been obtained in recent years, particularly by the work of Zaanen and Sawatzky,[6,7] who have pointed out how the presence of the insulating gap in these systems is related to a delicate balance among the Hubbard U and charge transfer Δ energies, and the widths w and W of the metal d and oxygen p bands, respectively. Both U (energy of the $d_i^n d_j^n \rightarrow d_i^{n-1} d_j^{n+1}$ process) and Δ (process $d_i^n \rightarrow d_i^{n+1}\underline{L}$, where $\underline{L}$ is a hole in the anion p band) originate from exchange and correlation effects, and are thus responsible for the breakdown of the independent electron model of Bloch band theory. The UHF method, as is well known, takes into account the spin-only electron correlation (exchange effect) exactly, while it neglects the spin-independent correlation. On the other hand, both correlation effects are accounted for, but at an approximate level, by the DFT-LSDA approach. Thus each of the two methods, from different starting points, may model usefully the deviations from one-electron theory. In particular, the larger the contribution of exchange to total electron correlation, the more convenient the UHF approach. One should keep in mind, however, that energy gaps are overestimated and underestimated by UHF and DFT results, respectively.

Following our previous work on iron and chromium sesquioxides, we have undertaken a study of the two early terms in the series of corundumlike first-row transition-metal oxides, Ti_2O_3 and V_2O_3. The first aim of this investigation is assessing the type of results given by the UHF method for systems much more difficult to deal with, in principle, because the early-row atoms Ti and V have very diffuse d orbitals with a tendency to delocalized bonding and metallic behavior. Second, it seems attractive to compare the electronic and chemical bonding properties throughout the whole first-row series of corundumlike oxides. Topics such as the amount of charge transfer from the ideal O^{2-} to Me^{3+} ion and of the associated spin polarization need to be characterized as a function of the number of d electrons of the transition metal, taking also into account the structural peculiarities of the corundum arrangement. Further, important related and long-debated questions concern the passage from charge-transfer to Mott-Hubbard insulating properties moving backwards along the row,[6,8] and the characterization of spin states and magnetic properties of these compounds.

A peculiar feature of titanium and vanadium sesquioxides are their phase transitions related to change of electronic behavior. Their room-temperature crystal structure has $R\bar{3}c$ space group, with a short Me-Me′ interatomic vector parallel to **c** (hexagonal setting), and a longer one Me-Me″ nearly parallel to the (001) basal plane. The Me atomic d states are split by the trigonal crystal field into an a_{1g} orbital and two pairs of doubly degenerate e_g^{π} and e_g^{σ} orbitals (Fig. 1). Hereafter, we shall often refer to the breaking of t_{2g} degeneracy by the rhombohedral field (with the ensuing occupation pat-

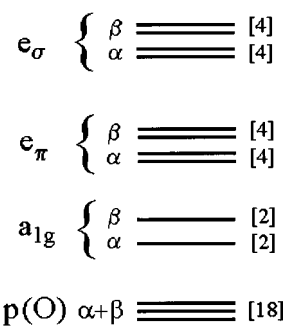

FIG. 1. Sketch of the electron energy level sequence for the isolated Me^{3+} ion in the trigonally distorted octahedral ligand field of the corundum structure. Possible exchange (α/β spin) splittings are included. The numbers of electrons which can be hosted (per Me_2O_3 unit) are indicated in square brackets.

tern of a_{1g} and e_g^π levels) as ''orbital ordering.''[9] The a_{1g} orbital is parallel to the **c** direction, and thus has the correct symmetry to form a covalent Me-Me′ bond; the e_g^π ones have directions close to the Me-Me″ contacts, while the e_g^σ orbitals are directed along the Me-O octahedral bonds. The Ti_2O_3 structure evolves in the 300–868-K temperature range[10] without symmetry changes, but with a sharp increase of the c/a ratio between 390 and 450 K. Above that temperature a broad transformation (about 200 K wide) from insulating to conducting behavior begins. This phenomenon was accounted for by the standard Goodenough's model[11,12] of band-crossing transition: on top of the valence band are the a_{1g} states occupied by one electron per Ti atom, and separated by a small gap (at room temperature) from the e_g^π, a_{1g}^* (antibonding), and e_g^σ bands present with increasing energy in the conduction band; with raising temperature, the gap between a_{1g} and e_g^π states is filled (band crossing) and metallic conductivity sets in. However, the exact nature of the transition is still controversial. Even the very structure of the valence band, which was traditionally interpreted as that of a typical Mott-Hubbard insulator on the basis of photoemission spectroscopic data,[13,14] has been recently questioned by new experiments[15] and suggested to be intermediate between Mott-Hubbard and charge transfer. Further, no conclusive indications are found in the literature about the magnetic behavior of Ti_2O_3 at low temperature, which is claimed to be antiferromagnetic[16] or nonmagnetic[17] by different authors on the basis of conflicting neutron diffraction experiments; yet diamagnetism seems to be more widely accepted. This point is very important, because the spin state inferred from magnetic properties affects also the electronic band structure: for instance, Goodenough's model is implicitly consistent with diamagnetism, but not with spin-polarized states. Theoretical results by a very recent DFT-LDA study[18] confirm the band sequence of the above model, but are unable to account for the energy gap in the room-temperature phase.

V_2O_3 is known to have metallic conductivity at room temperature, and to undergo a phase transition at 150 K to a monoclinic antiferromagnetic insulating phase.[19,20] However, the monoclinic structure (a slight distortion of the rombohedral one) is not considered in this work because it is computationally too demanding, and all calculations have been performed for the corundumlike arrangement only. Indeed, the insulating phase of V_2O_3 is stabilized in the rhombohedral structure at room temperature by Cr^{3+} doping.[21] Results from photoemission spectroscopy measurements[13,14] would indicate the e_g^π and a_{1g} states on top of the valence band. Further, recent data on optical conductivity[22,23] and corresponding theoretical analyses[24] would prove that the insulating gap of the low-temperature phase is really due to the Hubbard U energy. Similarly to Ti_2O_3, a central role in controlling the electronic properties is played by the c/a ratio, which is strongly related, in its turn, to metal-metal interatomic distances.[20] The metallic phase is characterized by a larger c/a value, with yet shorter Me-Me′ distances with respect to the insulating one: indeed, the c/a ratio of V_2O_3 at room temperature is outstandingly large by comparison to all other Me_2O_3 corundumlike oxides. A DFT-LDA simulation[25] found a plain conducting state with no indications for the opening of an energy gap, so that the metal-to-insulator transition was ascribed to a possible disordered or defect-type state.

Previous quantum-mechanical calculations on these compounds include a semiempirical tight-binding study[26] and another simplified linear combination of atomic orbitals (LCAO) treatment of V_2O_3 only, limited to d valence atomic orbitals.[27,28] The only modern, state-of-the art band structure studies are the two previously quoted DFT-LAPW calculations.[18,25]

II. COMPUTATION

All calculations were performed with the CRYSTAL92 code,[29] based on *ab initio* periodic Hartree-Fock methods with localized atomiclike basis functions (LCAO). The supplementary option for unrestricted treatment of the spin-dependent part of the wave function in open-shell systems was used[30] in order to obtain spin-polarized eigenfunctions of the Fock Hamiltonian, taking into account that the electronic configurations of isolated Ti^{3+} and V^{3+} ions are $1s^2 2s^2 2p^6 3s^2 3p^6 3d^1$ and $1s^2 2s^2 2p^6 3s^2 3p^6 3d^2$, respectively. The radial factors of atomic orbitals are expressed as linear combinations of Gaussian-type functions of the electron-nucleus distance. The all-electron basis sets used are very similar to those employed for the previous Cr_2O_3 and Fe_2O_3 calculations, with the O and Me (Ti or V) atoms represented by 18 and 27 atomic orbitals, respectively. The Gaussian basis set is of type 8-411G* (Ref. 31) for oxygen, and is reported in detail in a paper on α-Al_2O_3 (Ref. 32), except for the $4sp$ and $3d$ exponents, which were optimized to 0.214 (0.213) and 0.35 (0.35) by minimizing the total energy of the Ti_2O_3 (V_2O_3) crystal. The transition-metal atoms are represented by 8-6-411G contractions with two d-type (41G) shells. At first the Gaussian parameters were optimized by minimizing the energy of the isolated Ti^{3+} and V^{3+} ions. Then the exponents of the outermost $5sp$ and $4d$ shells were refined by searching for the minimum total energy of the Ti_2O_3 and V_2O_3 crystals at the experimental structural configuration. The optimized parameters are reported in Table I, and interpolate very well between those of the series of first-row transition-metal atoms determined in previous studies.

TABLE I. Exponents ($bohr^{-2}$) and contraction coefficients of the (individually normalized) Gaussian functions adopted for titanium and vanadium in the present study. $y[\pm z]$ stands for $y\times10^{\pm z}$.

Shell	Ti			V		
type	Exponents	Coefficients		Exponents	Coefficients	
		s	p,d		s	p,d
$1s$	1.972[+5]	2.690[−4]		2.222[+5]	2.590[−4]	
	2.940[+4]	2.110[−3]		3.300[+4]	2.050[−3]	
	6.550[+3]	1.140[−2]		7.282[+3]	1.126[−2]	
	1.791[+3]	4.858[−2]		1.963[+3]	4.900[−2]	
	5.616[+2]	1.589[−1]		6.078[+2]	1.621[−1]	
	1.978[+2]	3.557[−1]		2.124[+2]	3.623[−1]	
	7.572[+1]	4.233[−1]		8.097[+1]	4.217[−1]	
	2.992[+1]	1.481[−1]		3.203[+1]	1.392[−1]	
$2sp$	6.043[+2]	−4.880[−3]	8.590[−3]	6.488[+2]	−5.200[−3]	8.600[−3]
	1.447[+2]	−5.970[−2]	6.170[−2]	1.556[+2]	−6.270[−2]	6.170[−2]
	4.737[+1]	−1.338[−1]	2.317[−1]	5.104[+1]	−1.333[−1]	2.286[−1]
	1.795[+1]	2.370[−1]	4.746[−1]	1.946[+1]	2.497[−1]	4.581[−1]
	7.401[+0]	6.719[−1]	4.704[−1]	8.116[+0]	6.786[−1]	4.371[−1]
	2.936[+0]	2.529[−1]	1.484[−1]	3.279[+0]	2.529[−1]	1.484[−1]
$3sp$	2.643[+1]	4.480[−3]	−2.790[−2]	3.058[+1]	5.820[−3]	−2.650[−2]
	9.092[+0]	−4.615[−1]	−8.270[−2]	1.045[+1]	−4.192[−1]	−8.370[−2]
	4.229[+0]	−8.787[−1]	2.305[−1]	4.959[+0]	−8.673[−1]	2.210[−1]
	1.962[+0]	1.002[+0]	1.063[+0]	2.260[+0]	9.393[−1]	1.044[+0]
$4sp$	9.465[−1]	1.0[+0]	1.0[+0]	1.040[+0]	1.0[+0]	1.0[+0]
$5sp$	4.117[−1]	1.0[+0]	1.0[+0]	4.346[−1]	1.0[+0]	1.0[+0]
$3d$	2.329[+1]		3.079[−2]	2.341[+1]		3.962[−2]
	6.313[+0]		1.582[−1]	6.318[+0]		1.950[−1]
	2.112[+0]		3.883[−1]	2.099[+0]		4.320[−1]
	7.478[−1]		4.839[−1]	7.331[−1]		4.684[−1]
$4d$	2.667[−1]		1.0[+0]	2.696[−1]		1.0[+0]

The level of numerical approximation in evaluating the Coulomb and exchange series appearing in the self-consistent field (SCF) equations for periodic systems is controlled by five tolerances.[29] These are related to estimates of overlap or penetration for integrals of Gaussian functions on different centers, which define cutoff limits for series summation. The values used in the present calculations are 10^{-6}, 10^{-6}, 10^{-6}, 10^{-7}, and 10^{-13}, which correspond to severe computational conditions. The reciprocal space was sampled according to a regular sublattice defined by 32 points in the irreducible Brillouin zone, and convergence in the self-consistent-field cycles was controlled by a threshold $\Delta E=10^{-5}$ hartree per primitive unit cell.

Calculations were carried out both with ferromagnetic (FM) and antiferromagnetic (AF) spin arrangements, within the UHF computational scheme. In the former case the nonmagnetic space group $R\bar{3}c$ is preserved (all four Me atoms in the unit cell are symmetry related with aligned α electron spins); the number of n_α-n_β electrons in the unit cell was kept fixed to four (Ti_2O_3) or eight (V_2O_3) in the first SCF cycles, and it did not change significantly when this condition was relaxed (cf. the Mulliken population data reported below). In the AF configurations, two of the four Me atoms have a positive n_α-n_β spin density, and two have a negative one with equal absolute value, so as to produce a net vanishing n_α-n_β density in the unit cell. The symmetry is reduced to one of the three subgroups $R\bar{3}c$, $R\bar{3}$, and $R32$ of space group $R\bar{3}c$, giving rise to three alternative spin sequences along the threefold axis: $+-+-$ (AF1), $+--+$ (AF2), and $++--$ (AF3), respectively.[3]

In order to accelerate the slow convergence of SCF cycles for spin-polarized insulating states, the level shifter technique[33,34] was often employed: this enhances the energy difference between highest occupied and lowest empty states in the first cycles. Another feature used in the computations is based on shifting, by an arbitrary energy, the diagonal components of the Fock matrix corresponding to selected atomic orbitals at the starting cycle of the SCF procedure: in this way, one may try to force the SCF convergence to the absolute energy minimum, overcoming local minima or pseudosolutions. By the latter name we shall denote hereafter solutions of the SCF equations for which convergence is attained, but the energy is not minimum.

Restricted Hartree-Fock (RHF) and restricted open-shell Hartree-Fock (ROHF) calculations were also attempted, in order to simulate a fully diamagnetic crystal (vanishing n_α-n_β in each electron shell) and a spin-polarized crystal whose wave function is an eigenfunction of the spin moment operator $\hat{S}^2$ (in addition to S_Z), respectively. The contribution of electron correlation to the total energy, neglected in the Hartree-Fock approximation, was evaluated in some cases by an *a posteriori* scheme based on correlation-only density-functional formulas.[35]

TABLE II. Total energies per formula unit (hartree) for the ferromagnetic (FM), antiferromagnetic (AF), and diamagnetic (RHF) phases of Ti_2O_3 and V_2O_3, computed for the experimental crystal structures ($c/a = 2.639$ and 2.828, respectively) and for deformed unit cells. The values denoted by ''a'' correspond to conducting or semiconducting SCF solutions, the other ones to insulating states.

	Ti_2O_3			V_2O_3	
c/a	2.500	2.639	2.900	2.574	2.828
E (FM)		−1921.9346(I)	−1921.9305(I)	−2110.7910	−2110.8015
	−1921.7315(II)[a]		−1921.7566(III)[a]		
E (AF)		−1921.9412	−1921.9325	−2110.6725	−2110.8018
				−2110.5535[a]	
E (RHF)	−1921.8064	−1921.7947	−1921.7585	−2110.6137	−2110.6080
					−2110.2705[a]
ΔE (AF-FM)		−0.0066	−0.0020	0.1185	−0.0003
ΔE (RHF-FM)		0.1399	0.1720	0.1773	0.1935
	−0.0749(II)		−0.0019(III)		0.5310

III. RESULTS AND DISCUSSION

A. Ti_2O_3

The experimental crystal structure at room temperature[10] was used in all calculations aimed at characterizing the electronic and magnetic properties. As reported in Table II, a lower energy was obtained for the AF with respect to the FM spin arrangement, consistent with previous results for Fe_2O_3 and Cr_2O_3. In particular, the AF2 and AF1 spin sequences have very similar stabilities (−1921.9412 and −1921.9410 hartree, respectively), while the third arrangement (AF3) is much less stable. On the other hand, the energy value corresponding to the RHF solution is substantially higher than those of all UHF states, as expected in this type of calculation,[30] while convergence was not attained in attempts to obtain ROHF solutions. Thus it is hard to assess quantitatively the relative stability of antiferromagnetic and diamagnetic states of Ti_2O_3 by the present methods.

The total density of electronic states (DOS) and its projection onto the O contribution are shown in Fig. 2 for the FM structure (the AF result is quite similar). Figure 3 shows the Ti projected DOS's for the FM, AF, and RHF spin configurations. In the FM and AF cases, the triply degenerate $(t_{2g})^{\alpha}$ levels of Ti appear clearly to split into an $(a_{1g})^{\alpha}$ and two degenerate $(e_g^{\pi})^{\alpha}$ states, because of trigonal symmetry [the same occurs for $(t_{2g})^{\beta}$ levels]. This symmetry classification refers to the Γ point ($\mathbf{K}=0$) only. The a_{1g} band is narrower and higher in the AF than in the FM case. By the absence of antibonding $(a_{1g}^*)^{\alpha}$ states in the conduction band, a nonbonding character is inferred for the $(a_{1g})^{\alpha}$ peak. Its position just below the Fermi level at higher energy than the p(O) band indicates the electronic behavior of a Mott-Hubbard insulator, and agrees with experimental results of photoemission spectroscopy.[13,15] However, the a_{1g} and p(O) bands are in contact (Figs. 3 and 4), unlike the LAPW results,[18] showing a wide gap in between; this is consistent with the recent suggestion[15] that the electronic character of Ti_2O_3 could be intermediate between the Mott-Hubbard and charge-transfer insulators. The content of the a_{1g} peak is about one α electron per Ti atom, as shown by the Mulliken population analysis (Table III and IV). At the bottom of the conduction band the nonbonding $(e_g^{\pi})^{\alpha}$ states are observed, separated by a small gap from the antibonding $(e_g^{\sigma *})^{\alpha}$ ones. A small bonding $(e_g^{\sigma})^{\alpha}$ and $(e_g^{\sigma})^{\beta}$ contribution is superposed to the large p(O) band just below the $(a_{1g})^{\alpha}$ peak, corresponding to about 0.7 electron equally contributed by α and β spins (Table III). This $0.7e$ makes up the $\alpha+\beta$ electron transfer from the oxide ion O^{2-} to Ti^{3+}, similarly to what is observed for Cr_2O_3 (Ref. 3). It is interesting to remark that one electron per Ti atom is fully spin polarized (α state), corresponding to the ideal Ti^{3+} electronic configuration, while the excess 0.7 electron transferred from oxygen is not polarized.

In the nonmagnetic insulating RHF case the energy gap is smaller than for the spin-polarized solutions, and it is bracketed by an $a_{1g}(\alpha+\beta)$ bonding and an $a_{1g}^*(\alpha+\beta)$ antibond-

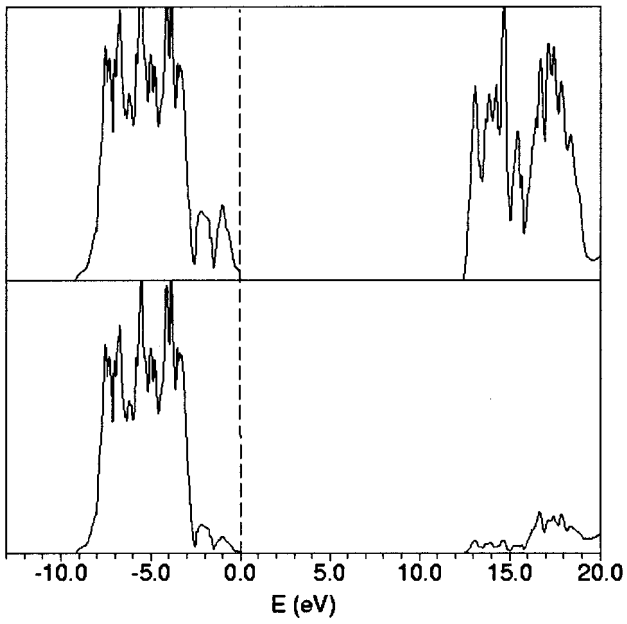

FIG. 2. Density of electronic states (DOS) of ferromagnetic Ti_2O_3 at $c/a = 2.639$ (experimental value). Total density and projection onto O states are shown above and below, respectively. The Fermi level is assumed at the energy zero.

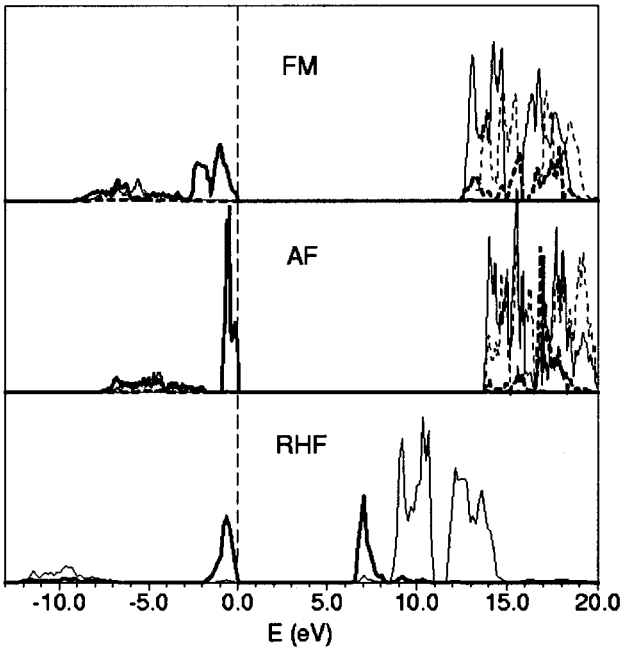

FIG. 3. Projection onto Ti states of the DOS of Ti_2O_3 ($c/a = 2.639$) for the insulating ferromagnetic, antiferromagnetic, and nonmagnetic (restricted Hartree-Fock) spin configurations. In the FM and AF cases, full and dashed lines denote α and β spins, respectively; in the RHF case, $\alpha+\beta$ spins are always meant (but the scale factor is 0.5). Thick and thin lines correspond to a_{1g} and e_g states, respectively.

ing peak, while the e_g^{π} peaks are located at higher energies in the conduction band. It should also be remarked that each electron state has double occupancy ($\alpha+\beta$) with respect to those (either α or β) appearing in the FM and AF cases.

During the SCF iterative procedure for solving the UHF equations in the FM case, at first a conducting pseudosolution (II) appears; it then gradually evolves into the much more stable insulating solution (I) (Table II). To interpret this result, we studied the effect of changing the c/a ratio

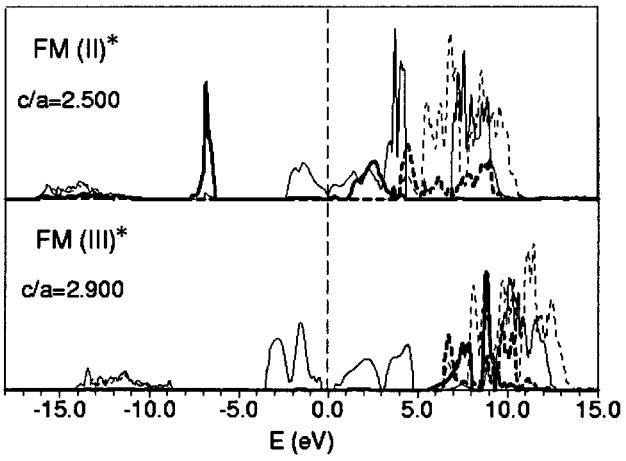

FIG. 4. Projection onto Ti states of the DOS of conducting (II) or semiconducting (III) pseudosolutions of ferromagnetic Ti_2O_3 at different c/a values. Symbols as in Fig. 3.

(keeping the unit-cell volume constant) on the electronic properties of the ferromagnetic UHF wave function, taking also into account that the transition to the conducting state occurs experimentally along with an increase of c/a with respect to the room-temperature ratio (2.64). At first the small value 2.50 was considered, obtaining full convergence for the conducting solution (II). Its DOS is shown in Fig. 4, and the corresponding Mulliken population data appear in Table IV. The $(a_{1g})^{\alpha}$ band is now split into two peaks, corresponding to bonding and antibonding Ti-Ti metal states, the lower of which belongs to the valence band and is occupied by about half electron per Ti atom, while the other one is located in the conduction band and is empty. The half electron left goes into the $(e_g^{\pi})^{\alpha}$ levels just below the Fermi energy. Metallic conductivity is triggered by promotion of electrons from $(e_g^{\pi})^{\alpha}$ to neighboring $(e_g^{\pi *})^{\alpha}$ and $(a_{1g}^{*})^{\alpha}$ antibonding states above E_F. It should be noticed that a significant bond overlap population is observed for the shortest Ti-Ti′ bond (Table IV), but that of the longer Ti-Ti″ bond lying in the basal plane is much smaller. This shows that in this pseudosolution an effective overlap of $(a_{1g})^{\alpha}$ orbitals along **c** is achieved, so as to promote Ti-Ti′ metal bonding. That state is expected to be stabilized at low c/a, because a short c edge favors the Ti-Ti′ metal bonding. However, its high energy (Table II) indicates that it is again a pseudosolution of the SCF equations. We tried to force convergence of the insulating solution by using the option mentioned in Sec. II, but without success.

At $c/a \geqslant 2.90$, the SCF cycles converged to a third type of solution (III), with energy comparable to that of phase II (Table II). This solution is nearly metallic (actually, semiconducting with a very small energy gap), and corresponds to an inversion of the relative energies of the $(a_{1g})^{\alpha}$ and $(e_g^{\pi})^{\alpha}$ bands with respect to solution I, as can be seen from the DOS of Fig. 4, achieving a configuration resembling that of V_2O_3 (cf. below). The lower half of the $(e_g^{\pi})^{\alpha}$ band is occupied by about one electron per Ti atom (Table III). A tendency to metal bonding in the basal plane, unlike the case of phase II, is indicated by the significant Ti-Ti″ bond overlap population, and is clearly related to the short a cell edge. However, this is actually a pseudosolution as for case II: by using the computational option referred to above, and forcing the energy of the $a_{1g}(d_z^2)$ orbital of Ti to be very low at the first SCF cycle, the ''regular'' solution I was obtained with a much lower energy (Table II). We point out that *a posteriori* corrections for the neglect of correlation effects do not change significantly the relative values of total energies reported in Table II.

The results here obtained differ substantially from both the classical Goodenough's model[11] and the recent LAPW calculation[18] of Ti_2O_3, which is consistent with that model except for being unable to reproduce the band gap opening in the insulating state. In both cases[11,18] the DOS shows a bonding a_{1g} and an antibonding a_{1g}^{*} band with the e_g^{π} one in between, resembling somehow our RHF solution except for the lower location of the e_g^{π} band; accordingly, no mention is made of spin polarization or distinction between α and β electron states. On the other hand, our stable UHF (FM or AFM) insulating solution (I) implies no $(a_{1g})^{\alpha}/(a_{1g}^{*})^{\alpha}$ splitting, but a single nonbonding $(a_{1g})^{\alpha}$ band, due evidently to

TABLE III. Mulliken population data of electron charge distribution for Ti_2O_3 and V_2O_3 (this study), and for Cr_2O_3 (Ref. 3) and Fe_2O_3 (Ref. 2). Results concern α and β spins related to metal (Me) atomic orbital shells and Me-O bond overlap for the antiferromagnetic (AF) configuration, and $\alpha+\beta$ and $\alpha-\beta$ overall metal and oxygen populations for the ferromagnetic (FM) case.

	Ti_2O_3		V_2O_3		Cr_2O_3		Fe_2O_3	
AF	α	β	α	β	α	β	α	β
Me								
a_{1g}	0.984	0.042	0.053	0.043	0.995	0.030	0.099	0.028
e_g^π	0.083	0.075	1.969	0.073	1.985	0.055	1.992	0.044
Total t_{2g}	1.066	0.116	2.021	0.115	2.980	0.085	2.991	0.072
e_g^σ	0.280	0.254	0.346	0.270	0.324	0.227	2.020	0.213
Total d	1.346	0.370	2.367	0.385	3.303	0.311	5.011	0.285
Grand total	10.379	9.392	11.415	9.414	12.345	9.330	14.062	9.320
Net charge	+2.229		+2.171		+2.325		+2.618	
Me-O′	0.014	0.018	0.012	0.021	0.010	0.016	−0.014	0.019
Me-O″	0.002	0.008	0.008	0.014	0.007	0.012	−0.005	0.012
FM	$\alpha+\beta$	$\alpha-\beta$	$\alpha+\beta$	$\alpha-\beta$	$\alpha+\beta$	$\alpha-\beta$	$\alpha+\beta$	$\alpha-\beta$
Me	19.769	1.003	20.829	2.012	21.677	3.023	23.383	4.745
O	9.487	−0.002	9.447	−0.008	9.549	−0.015	9.745	0.170

insufficient Ti-Ti′ electron overlap. That splitting is present in the conducting pseudosolution II, with a partial overlap of $(a_{1g}^*)^\alpha$ and $(e_g^\pi)^\alpha$ bands.

The gradual transition to a conducting state, accompanied by an increase of c/a, should be ascribed to the $(a_{1g})^\alpha$ and $(e_g^\pi)^\alpha$ bands merging into a single one (band crossing) according to Goodenough's model. Hartree-Fock results at very large c/a, showing the appearance of the pseudosolution III, would indicate the final state of the process, characterized by full inversion of the $(a_{1g})^\alpha$ and $(e_g^\pi)^\alpha$ positions on the energy scale with the Fermi level in the middle of the $(e_g^\pi)^\alpha$ band. We can thus summarize this qualitative UHF model of Ti_2O_3 as follows: (i) at the room-temperature c/a value, the insulating state shows an occupied, fully spin-polarized nonbonding $(a_{1g})^\alpha$ band at the top of the valence states. No Ti-Ti′ antibonding levels appear in the conduction band. (ii) The transition to a conducting state is due to the increase of c/a, which implies a destabilization of $(a_{1g})^\alpha$ with respect to the $(e_g^\pi)^\alpha$ band, and ends up by exchanging their energies. The doubly degenerate $(e_g^\pi)^\alpha$ band is filled by one electron per Ti atom, giving rise to metallic behavior. Such a model is, however, quantitatively unsatisfactory because the relative energies of solutions I and III at large c/a are not correct, and because the antiferromagnetic configuration, though more stable, does not reveal any of the relevant features apparent in the FM case.

The structural variables of the corundum atomic arrangement in the case of Ti_2O_3 [a and c hexagonal cell edges, x(O) and z(Ti) atomic fractional coordinates] were also optimized by searching for the least-energy configuration. In Table V all results are reported, showing that the positive error for the unit-cell volume is slightly larger than that obtained for Cr_2O_3 (+5.2%); the c/a ratio, on the other hand, is reproduced with a good approximation.

B. V_2O_3

The ground-state total energy was computed for the room-temperature rhombohedral structure[21] ($c/a=2.828$) with

TABLE IV. Mulliken population data of electron charge distribution for three ferromagnetic UHF-SCF solutions for Ti_2O_3: stable insulating configuration (I), conducting pseudosolution (II), and semiconducting pseudosolution (III).

	Ti_2O_3 (I)		Ti_2O_3 (II)		Ti_2O_3 (III)	
FM	α	β	α	β	α	β
Ti						
a_{1g}	0.995	0.034	0.531	0.036	0.062	0.039
e_g^π	0.079	0.074	0.546	0.079	1.036	0.070
Total t_{2g}	1.074	0.108	1.077	0.115	1.097	0.109
e_g^σ	0.281	0.253	0.299	0.253	0.301	0.251
Total d	1.354	0.360	1.376	0.368	1.398	0.360
Ti-O′	0.013	0.018	0.016	0.019	0.017	0.018
Ti-O″	0.002	0.008	0.009	0.010	0.011	0.010
Ti-Ti′	−0.002	−0.001	0.039	−0.001	−0.003	0.000
Ti-Ti″			0.008	0.001	0.014	0.000

TABLE V. Calculated (least-energy) and experimental equilibrium values (see the text for references) of hexagonal unit-cell edges, volume per formula unit, atomic fractional coordinates, Me-O distances for corundumlike Ti_2O_3 and V_2O_3. Percentage errors are indicated. Energies of the optimized structures are reported too.

	Ti_2O_3		V_2O_3	
	Calc.	Expt.	Calc.	Expt.
a_0	5.293(+2.6%)	5.157	5.138(+3.8%)	4.949 Å
c_0	13.859(+1.8%)	13.610	13.947(−0.4%)	13.998 Å
c_0/a_0	2.618(−0.8%)	2.639	2.715(−4.0%)	2.828
V_0	336.2(+7.3%)	313.5	318.9(+7.4%)	296.9 Å^3
x (O)	0.30075	0.3133	0.3006	0.3122
z (Me)	0.35400	0.34485	0.3534	0.3463
Me-O′	2.050(+1.2%)	2.025	2.007(+2.0%)	1.969 Å
Me-O″	2.147(+3.8%)	2.068	2.113(+3.1%)	2.051 Å
E_{min} (hartree)	−1921.9495		−2110.8175	

three different spin configurations, similarly to Ti_2O_3: diamagnetic closed-shell (RHF), ferromagnetic (UHF-FM), and antiferromagnetic (UHF-AF) open-shell (Table II). A slight preference for antiferromagnetism versus ferromagnetism is shown by the calculations, in accordance with results for all other corundumlike sesquioxides. In particular, for this compound the AF3 ($R32$) spin configuration is predicted to be slightly more stable than the AF1 ($R3c$) one, while the AF2 structure is less stable than the ferromagnetic one. The ΔE (AF-FM) energy is −0.0003, −0.0001, and +0.0006 hartrees for the three cases, respectively. The closed-shell solution is insulating just as the two spin-polarized ones, and it shows a positive energy difference with both of them, which is larger than the ΔE (RHF-FM) value observed for Ti_2O_3. This might indicate that diamagnetism is very unfavorable for V_2O_3. Further, in the present case a closed-shell pseudosolution is obtained as well, denoted as RHF* and characterized by an even higher energy.

The total DOS of the insulating FM solution is shown in Fig. 5, while the projections onto vanadium states for all three cases FM, AF, and RHF appear in Fig. 6. The FM and AF valence bands are built up by a superposition of p(O) and $(e_g^\pi)^\alpha$(V) states in the same energy range, while a_{1g}, e_g^σ, and $(e_g^\pi)^\beta$ vanadium states are observed in the lower part of the conduction band. An appreciable density of $(e_g^\sigma)^\alpha$ and $(e_g^\sigma)^\beta$ states is also present, however, within the valence band, corresponding to V-O covalent bonding. The Mulliken population analysis (Table III) shows that the $(e_g^\pi)^\alpha$ states are occupied by about two electrons per V atom, while most of the charge transfer from O^{2-} to V^{3+} concerns $(e_g^\sigma)^{\alpha+\beta}$ levels, just as for Ti_2O_3 and Cr_2O_3. On the other hand, a very different band occupation scheme appears for the RHF state shown in Fig. 6. This resembles strikingly that of the FM and AF insulating solutions of Ti_2O_3 (Fig. 3), with the a_{1g} levels on top of the valence band below the empty e_g^π states. Such a scheme is made possible by the a_{1g} levels hosting two $\alpha+\beta$ electrons per V atom in the closed-shell configuration, instead of a single (either α or β) one as in the open-shell cases. The reverse situation is shown in the DOS of the RHF* pseudosolution (Fig. 7), with the e_g^π states below the a_{1g} ones, but in this case the Fermi level falls in the middle of the e_g^π band, which can host four electrons per V atom because of double occupancy ($\alpha+\beta$) of each state. Thus nearly metallic (semiconducting with a very small energy gap) behavior ensues.

Taking into account the results obtained for Ti_2O_3, the effect of distorting the c/a ratio on the electronic structure of V_2O_3 was studied by considering the $c/a=2.574$ value. A compression of the c edge of the hexagonal cell is expected to lower the energy of the a_{1g} levels, thus decreasing the insulating gap and favoring metal conductivity. Actually in the first SCF cycles of the FM state a metallic solution appears, where the $(e_g^\pi)^\alpha$ and $(a_{1g})^\alpha$ bands touch at the Fermi energy; however, soon the energy drops by about 0.2 har-

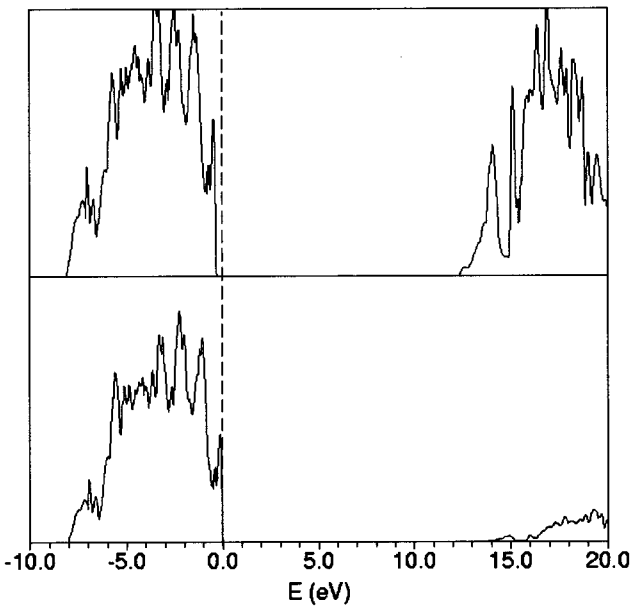

FIG. 5. Density of electronic states (DOS) of ferromagnetic V_2O_3 at $c/a=2.828$ (experimental value). Total density and projection onto O states are shown above and below, respectively. The Fermi level is assumed at the energy zero.

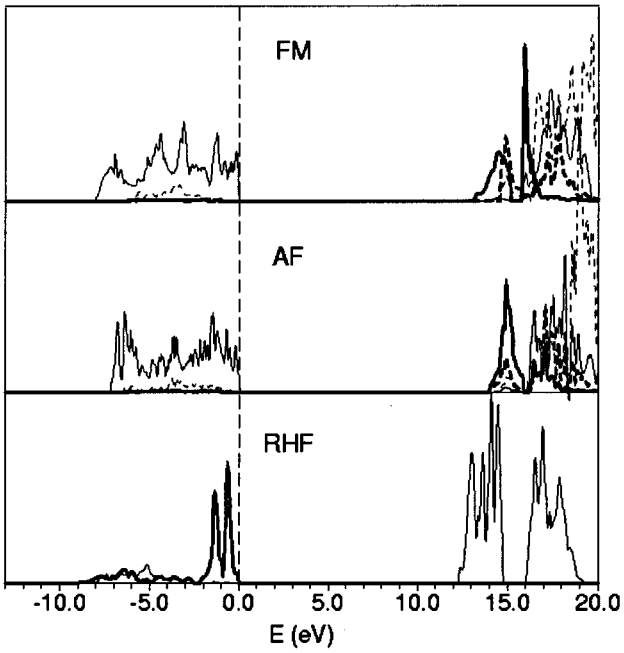

FIG. 6. Projection onto V states of the DOS of V_2O_3 ($c/a = 2.828$) for the insulating ferromagnetic, antiferromagnetic and non-magnetic (restricted Hartree-Fock) spin configurations. In the FM and AF cases, full and dashed lines denote α and β spins, respectively; in the RHF case, $\alpha+\beta$ spins are always meant (scale factor 0.5). Thick and thin lines correspond to a_{1g} and e_g states, respectively.

trees per formula unit and the usual insulating solution is stabilized. The effect is even larger for the antiferromagnetic case, which converges straightforwardly to a conducting state AF* with the $(a_{1g})^{\alpha}$ band below $(e_g^{\pi})^{\alpha}$, and the Fermi energy in the middle of the $(e_g^{\pi})^{\alpha}$ band (Fig. 7). However, that is actually a pseudostate, and convergence to the stable insulating solution can be forced by the usual procedure (cf. Table II). The previous DFT-LAPW study of V_2O_3 (Ref. 25) invariably gave a metallic state with overlapping $(e_g^{\pi})^{\alpha}$ and

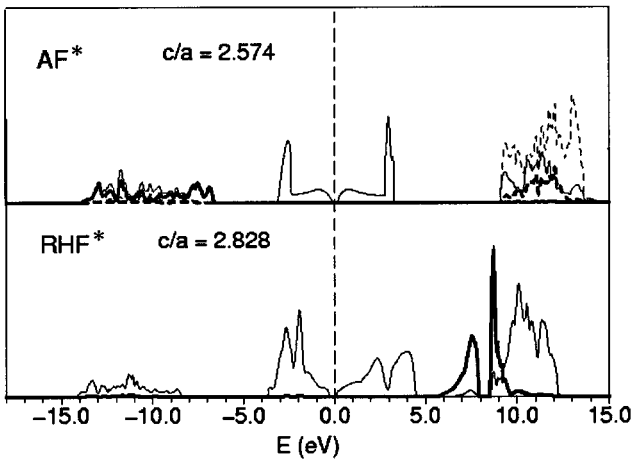

FIG. 7. Projection onto V states of the DOS of conducting or semiconducting pseudosolutions of V_2O_3 at different c/a values. Symbols as in Fig. 3.

$(a_{1g})^{\alpha}$ bands at the Fermi level, in a similar way to the other calculation on Ti_2O_3 (Ref. 18). Thus, the insulating phases of both compounds cannot be reproduced by the state-of-the-art DFT-LDA method, while UHF results not only give stable insulating states, but also account somehow for the conducting phases by means of higher-energy pseudosolutions. This different behavior might suggest that spin-only correlation effects play a major role in the breaking of the one-electron approximation for these compounds.

A structural optimization was carried out for V_2O_3, similarly to Ti_2O_3. The results (Table V) show a larger overestimate of the a cell edge, while the c edge is reproduced more accurately; thus the negative error for the c/a ratio is much larger than in the Ti_2O_3 case. This confirms the peculiar large value of c/a for V_2O_3 in the series of corundumlike oxides.

C. Comparison with Cr_2O_3 and Fe_2O_3

The Mulliken electron populations of chromium and iron sesquioxides obtained in previous studies[2,3] are reported in Table III for comparison with those of the present compounds. Ti_2O_3, V_2O_3, and Cr_2O_3, have similar behavior, with $0.7-0.8|e|$ charge transfers from $\frac{3}{2}O^{2-}$ to Me^{3+}, while only $0.4|e|$ are transferred in the case of Fe_2O_3. Most of these electrons (over 90% and 77% in the two cases, respectively) go into the d shell, and the rest into the outer sp orbitals of Me^{3+}. A further, important difference between the first three oxides and Fe_2O_3 concerns the α/β spin ratio of electrons transferred to the metal d shell: all these electrons have β spin in the case of ferric oxide, because all d^{α} levels are filled for the ideal Fe^{3+} ion, while they are approximately divided into equal amounts of α and β spins for the group of other oxides. All of the α, and most of β, transferred electrons go into the e_g^{σ} levels; this is related to the covalent interaction with $p(O)$ states, leading to Me-O σ bond formation and bringing a fraction of $(e_g^{\sigma})^{\alpha}$ and $(e_g^{\sigma})^{\beta}$ states below the Fermi energy.

The type of spin polarization of transferred electrons (nearly vanishing for Ti, V, and Cr oxides, full β for Fe_2O_3) has remarkable consequences on the overall net spin moment $n_{\alpha}-n_{\beta}$ per metal atom. That is significantly lower than the ideal number of d electrons for Fe (4.745 versus 5), but is very close for Ti (1.003), V (2.012), and Cr (3.023), with even a slight excess increasing from Ti to Cr. In the ferromagnetic case, the deviation from the ideal value on the cation is compensated by an opposite deviation on the oxide ion, so as to produce very small β-type anion spin polarizations in Ti_2O_3, V_2O_3, and Cr_2O_3, and a larger α-type one in Fe_2O_3 (Table III). In the AF case, of course, these anion spin polarizations have signs matching those of the spin moments of neighboring cations. A clear picture of this phenomenon appears from spin density maps such as those of Figs. 8 and 9, and the similar ones appearing in Refs. 2 and 3. Figures 8 and 9 also show clearly the space distributions of the a_{1g} and e_g^{π} orbitals, respectively, which are occupied by one or two d electrons in the case of Ti_2O_3 or V_2O_3 in their spin-polarized insulating states.

It is also interesting to consider the Me-O bond overlap populations appearing in Table III. For Ti, V, and Cr, positive values are observed for α and β electrons, indicating a bonding interaction for both spin states (slightly larger for β

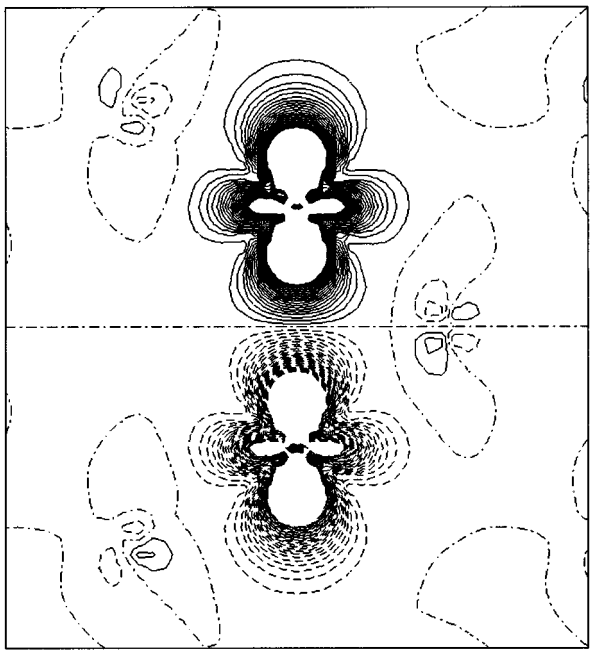

FIG. 8. Difference spin density (spin up minus spin down) maps on the (010) hexagonal plane for antiferromagnetic Ti_2O_3. Isodensity curves are separated by $0.20e$ Å^{-3}. Continuous, dashed-dotted, and dashed lines indicate positive, zero, and negative values, respectively.

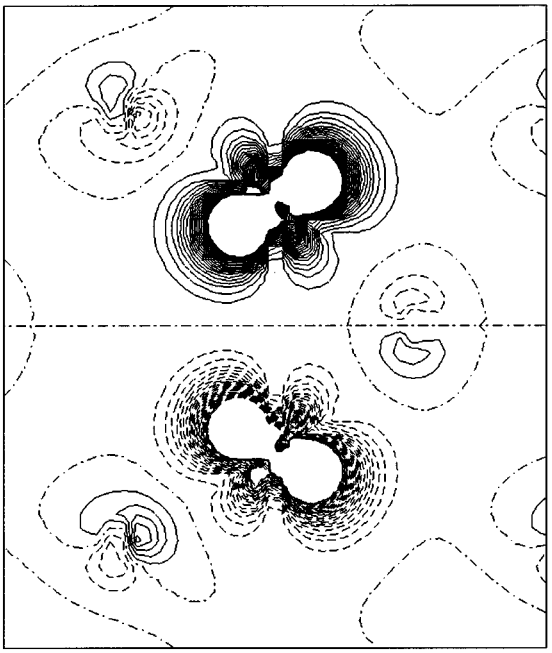

FIG. 9. Difference spin density (spin up minus spin down) maps on the (010) hexagonal plane for antiferromagnetic V_2O_3. Isodensity curves are separated by $0.20e$ Å^{-3}. Continuous, dashed-dotted, and dashed lines indicate positive, zero, and negative values, respectively.

spins). This corresponds to the $\alpha+\beta$ O^{2-} to Me^{3+} charge transfer discussed above. In the case of Fe, on the other hand, the overlap population is positive for β spin but negative for the α one, according to an antibonding repulsion of α electrons. The latter is due to the full d^{α} shell of Fe^{3+} exerting an exchange repulsion towards α electrons in the Fe-O region.

IV. CONCLUSIONS

The most stable SCF solutions of periodic Hartree-Fock equations for Ti_2O_3 and V_2O_3 correspond to spin-polarized insulating states with orbital ordering within the split t_{2g} levels: $E(a_{1g})<$ or $>E(e_g^{\pi})$ for Ti_2O_3 or V_2O_3, respectively. However, solutions with higher energy are also obtained, particularly at deformed unit-cell geometries, showing conducting or semiconducting behavior and different types of orbital ordering with respect to the previous ones. This contrasts with DFT-LDA calculations[18,25] on both compounds, which always give metallic states without accounting for the insulating phases. The UHF pseudosolutions obtained can be qualitatively related to the metal-insulator phase transitions observed in both oxides. In particular, the c/a ratio of unit-cell edges is proved to control closely the relative positions of t_{2g} bands and thus the kind of orbital ordering. In the Ti_2O_3 case, at large c/a ratios $E(e_g^{\pi})$ $<E(a_{1g})$ is obtained, so that the metallic state is accounted for by a single electron occupying a doubly degenerate band. Further, a considerable electron transfer from oxygen to metal ions ($0.7-0.8|e|$) is calculated, contributing to chemical bonding by partial occupation of e_g^{σ} bands. This effect is similar to that observed for Cr_2O_3, but is much larger than in the case of Fe_2O_3.

ACKNOWLEDGMENTS

The work was supported by the Human Capital and Mobility Programme of the European Union under Contract No. CHRX-CT93-0155, and by the Ministero Università e Ricerca Scientifica e Tecnologica, Roma.

*Present address: Dipartimento di Scienza dei Materiali, Università di Milano, via Emanueli 15, 20126 Milano, Italy.

[1] M. D. Towler, N. L. Allan, N. M. Harrison, V. R. Saunders, W. C. Mackrodt, and E. Aprà, Phys. Rev. B **50**, 5041 (1994).
[2] M. Catti, G. Valerio, and R. Dovesi, Phys. Rev. B **51**, 7441 (1995).
[3] M. Catti, G. Sandrone, G. Valerio, and R. Dovesi, J. Phys. Chem. Solids **57**, 1735 (1996).
[4] P. Dufek, K. Schwarz, and P. Blaha, Phys. Rev. B **48**, 12 672 (1993).
[5] P. I. Sorantin and K. Schwarz, Inorg. Chem. **31**, 567 (1992).
[6] J. Zaanen, G. A. Sawatzky, and J. W. Allen, Phys. Rev. Lett. **55**, 418 (1985).
[7] J. Zaanen and G. A. Sawatzky, J. Solid State Chem. **88**, 8 (1990).
[8] P. Kowalczyk, L. Ley, F. R. McFeely, and D. A. Shirley, Phys. Rev. B **15**, 4997 (1977).
[9] K. I. Kugel' and D. I. Khomskii, Usp. Fiz. Nauk. **136**, 621 [Sov. Phys. Usp. **25**, 231 (1982)].
[10] C. E. Rice and W. R. Robinson, Acta Crystallogr. B **33**, 1342 (1977).

[11] J. B. Goodenough, Prog. Solid State Chem. **5**, 145 (1972).
[12] P. A. Cox, *The Transition Metal Oxides* (Oxford University Press, Oxford, 1992).
[13] K. E. Smith and V. E. Henrich, Phys. Rev. B **38**, 5965 (1988).
[14] K. E. Smith and V. E. Henrich, Phys. Rev. B **38**, 9571 (1988).
[15] T. Uozumi, K. Okada, A. Kotani, Y. Tezuka, and S. Shin, J. Phys. Soc. Jpn. **65**, 1150 (1996).
[16] S. C. Abrahams, Phys. Rev. **130**, 2230 (1963).
[17] H. Kendrick, A. Arrott, and S. A. Werner, J. Appl. Phys. **39**, 585 (1968).
[18] L. F. Mattheiss, J. Phys. Condens. Matter **8**, 5987 (1996).
[19] R. M. Moon, Phys. Rev. Lett. **25**, 527 (1970).
[20] M. Yethiraj, J. Solid State Chem. **88**, 53 (1990).
[21] P. D. Dernier, J. Phys. Chem. Solids **31**, 2569 (1970).
[22] G. A. Thomas, D. H. Rapkine, S. A. Carter, A. J. Millis, T. F. Rosenbaum, and J. M. Honig, Phys. Rev. Lett. **73**, 1529 (1994).
[23] R. Raimondi, Phys. Rev. B **51**, 10 154 (1995).
[24] J. Hong and H. Y. Kee, Europhys. Lett. **33**, 453 (1996).
[25] L. F. Mattheiss, J. Phys. Condens. Matter **6**, 6477 (1994).
[26] J. Ashkenazi and T. Chuchem, Philos. Mag. **32**, 763 (1975).
[27] C. Castellani, C. R. Natoli, and J. Ranninger, Phys. Rev. B **18**, 4945 (1978).
[28] C. Castellani, C. R. Natoli, and J. Ranninger, Phys. Rev. B **18**, 4967 (1978).
[29] R. Dovesi, V. R. Saunders, and C. Roetti, *CRYSTAL92. User's Manual* (Gruppo di Chimica Teorica, Università di Torino, Torino, 1992).
[30] E. Aprà, thesis, University of Torino, 1993.
[31] W. H. Hehre, L. Radom, P. R. Schleyer, and J. A. Pople, *Ab Initio Molecular Orbital Theory* (Wiley, New York, 1986).
[32] M. Catti, G. Valerio, R. Dovesi, and M. Causà, Phys. Rev. B **49**, 14 179 (1994).
[33] V. R. Saunders and I. H. Hillier, Int. J. Quantum Chem. **7**, 699 (1973).
[34] M. F. Guest and V. R. Saunders, Mol. Phys. **28**, 819 (1974).
[35] J. P. Perdew, J. A. Chevary, S. H. Vosko, K. A. Jackson, M. R. Pederson, D. J. Singh, and C. Fiolhais, Phys. Rev. B **46**, 6671 (1992).